For $\zeta \to 0$ the expression for $\Phi_s(\zeta)$ is an indeterminacy of the type 0/0. Expanding this indeterminacy, we obtain

$$\Phi_s(0) = 2^{s+2} \int_0^1 dx\, x^{s+3} \left[(1-x^2)^{-1/2} - \operatorname{arch} \frac{1}{x} \right]. \tag{54}$$

In particular,

$$\Phi_0(0) = 4, \quad \Phi_{-2}(0) = 1, \quad \Phi_{-2}(0) = 0.$$

For $s = -4$ the integral in (54) diverges at the lower limit. The divergence in (54) implies that the first term of the asymptotic expansion of $\Phi_{-4}(\zeta)$ in $\zeta \ll 1$ is a nonanalytic function of ζ. Carrying out the asymptotic expansion of $\Phi_{-4}(\zeta)$ up to terms of zeroth order in ζ^2, we obtain

$$\Phi_{-4} = -1/2 \ln^2 \zeta + (2 \ln 2 - 1) \ln \zeta + C_1,$$

$$C_1 = 1/2 + 3/2 \ln 2 - \ln^2 2 - \frac{1}{2} \int_0^1 dx \left\{ x^{-1} \operatorname{arsh} x + x^{-1} \ln \frac{1}{2} [1 + (1+x^2)^{1/2}] \right.$$

$$\left. + 3x^{-1} \ln \frac{1}{2} [1 + (1-x^2)^{1/2}] + 2x^{-3} \left[(1-x^2)^{1/2} - 1 + \frac{1}{2} x^2 \right] \right\} \approx 0.78.$$

It follows from (55) that $\Phi_{-4}(\zeta) < 0$ when $\zeta < \zeta_0 \approx 0.4$.

The author is grateful to L. V. Keldysh for constant attention and valuable advice in the course of the work.

[1)]The formula (11a) is contained in the handbook.[15a] Its connection with the problem under consideration was first pointed out in[16].

[2)]The value $s = -3$ does not correspond to any real scattering mechanism.

[1]Ya. B. Zel'dovich and Yu. P. Raĭzer, Zh. Eksp. Teor. Fiz. 47, 1150 (1964) [Sov. Phys. JETP 20, 772 (1965)].
[2]An. V. Vinogradov, Zh. Eksp. Teor. Fiz. 68, 1091 (1975) [Sov. Phys. JETP 41, 540 (1975)].
[3]P. M. Mednis and V. M. Faĭn, Zh. Eksp. Teor. Fiz. 62, 812 (1972) [Sov. Phys. JETP 35, 429 (1972)].
[4]A. I. Rubinshteĭn and V. M. Faĭn, Fiz. Tverd. Tela 15, 470 (1973) [Sov. Phys. Solid State 15, 332 (1973)].
[5]A. S. Epifanov, Zh. Eksp. Teor. Fiz. 67, 1805 (1974) [Sov. Phys. JETP 40, 897 (1975)].
[6]D. Marcuse, Bell Syst. Techn. J. 41, 1557 (1962).
[7]T. Musha and F. Yoshida, Phys. Rev. A133, 1303 (1964).
[8]F. V. Bunkin and M. V. Fedorov, Zh. Eksp. Teor. Fiz. 49, 1215 (1965) [Sov. Phys. JETP 22, 844 (1966)].
[9]F. V. Bunkin, A. E. Kazakov, and M. V. Fedorov, Usp. Fiz. Nauk 107, 559 (1972) [Sov. Phys. Usp. 15, 416 (1973)].
[10]P. V. Elyutin, Zh. Eksp. Teor. Fiz. 65, 2196 (1973) [Sov. Phys. JETP 38, 1097 (1974)].
[11]M. V. Fedorov, Zh. Tekh. Fiz. 41, 849 (1971) [Sov. Phys. Tech. Phys. 16, 671 (1971)].
[12]V. L. Malevich and É. M. Épshteĭn, Kvantovaya Elektron, (Moscow) 1, 1468 (1974) [Sov. J. Quantum Electron. 4, 816 (1974)].
[13]É. M. Épshteĭn, Fiz. Tverd. Tela 11, 2732 (1969) [Sov. Phys. Solid State 11, 2213 (1970)].
[14]G. N. Watson, Theory of Bessel Functions, Cambridge University Press, Cambridge, Eng., 1944 (Russ. Transl., IIL, 1949).
[15]I. S. Gradshteĭn and I. M. Ryzhik, Tablitsy integralov, summ, ryadov i proizvedeniĭ (Tables of Integrals, Series, and Products), Nauka, 1971 (Eng. Transl., Academic Press, New York, 1965), a) 8.536, b) 2.598.
[16]A. S. Epifanov, A. A. Manenkov, and A. M. Prokhorov, Pis'ma Zh. Eksp. Teor. Fiz. 21, 483 (1975) [JETP Lett. 21, 223 (1975)].
[17]V. P. Silin, Zh. Eksp. Teor. Fiz. 47, 2254 (1964) [Sov. Phys. JETP 20, 1510 (1965)].

Translated by A. K. Agyei.

Low-temperature luminescence study of generation of normal acoustic waves in pure germanium under double injection conditions

M. S. Murashov, V. N. Ivanov, and A. P. Shotov

P. N. Lebedev Physics Institute, USSR Academy of Sciences, Moscow

(Submitted July 22, 1975)
Zh. Eksp. Teor. Fiz. **70**, 1009–1026 (March 1976)

An investigation of the spatial and temporal distributions of low-temperature luminescence emitted from rectangular pure germanium resonators under double injection conditions revealed generation of normal finite-amplitude acoustic waves. A strong interaction was observed between various modes of these normal waves, which resulted in their coupling. The interaction of the excited vibrations with the injected plasma deformed strongly the carrier energy spectrum, as manifested by a long-wavelength shift (by up to 6 meV) of exciton luminescence lines. A special feature of this generation mechanism was the accumulation of gain from pulse to pulse because of weak attenuation of sound at the generation frequencies. A limiting value of the gain was reached because of nonlinear effects.

PACS numbers: 72.30.+q, 72.80.Cw, 72.50.+b, 78.60.−b

Properties of semiconductors at high excitation rates are attracting considerable interest. The present investigation was intended to investigate, by the radiative recombination method, the properties of excitons created in high densities in pure germanium by double injection of carriers and the properties of the nonequilibrium state of the phonon system. Injection of nonequilibrium carriers in high densities was accompanied by the

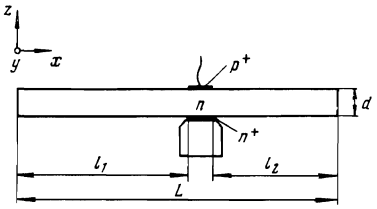

FIG. 1. Schematic representation of a sample.

evolution of a considerable energy which was transferred mainly to the lattice vibrations. The slow low-temperature relaxation of phonons, at least those with long wavelengths, could disturb their equilibrium. We showed earlier[1] that double injection in pure germanium at low temperatures resulted in a strong disequilibrium of the phonon system even in the range of the quasi-Brillouin TA phonons with $q \lesssim \pi/a$. Moreover, it was found that under these conditions the energy spectrum of carriers changed considerably as manifested by a 5–6 meV long-wavelength shift of the luminescence line maxima. This shift was attributed to the interaction of hot carriers with long-wavelength acoustic phonons.

In the present case we studied not only the evolution of the low-temperature luminescence emitted from $p^+ - n - n^+$ structures made of pure germanium but also the spatial distribution. We found that the latter was inhomogeneous. Not only the intensity but also the spectral positions of the luminescence lines and their widths varied with time and space producing a pattern of quasistanding waves. These oscillations were due to the existence of high-amplitude ultrasonic waves in $p^+ - n - n^+$ structures, generated as a result of amplification of normal vibrations of a crystal by a supersonic carrier flux. The deformation associated with these waves caused periodic fluctuations of the potential energy of carriers and their density, manifested by the space and time modulation of the luminescence spectrum. The observed long-wavelength shift of the luminescence lines depended periodically on the coordinate and time and was governed by the amplitude of the amplified acoustic waves. The maximum shift $\Delta E \sim 6$ meV was due to the saturation of the amplitude caused clearly by nonlinear effects.

An investigation of spatially resolved luminescence spectra established that the phonon disequilibrium effects, including the long-wavelength shift of the luminescence lines, were observed also at liquid nitrogen temperature.

EXPERIMENTAL METHOD

Luminescence (recombination radiation) was investigated in the temperature range 2–100 °K using $p^+ - n - n^+$ structures of different configurations made of pure n-type germanium with a net residual impurity concentration of 5×10^{12} and 5×10^{13} cm^{-3}, respectively. The electron- and hole-injecting n^+ and p^+ contacts were formed by alloying the original material with In + 2% As and In + 0.5% Ga. The distance between the contacts was varied between 0.15 and 0.85 mm.

In a more detailed investigation of the acoustic waves excited in $p^+ - n - n^+$ structures we used specially prepared samples in the form of slabs of different sections and length shown schematically in Fig. 1. We introduced, for convenience, a coordinate system with the z axis parallel to the current and x and y axes directed as shown in Fig. 1. We investigated samples with contacts separated by $d = 0.36$ and 0.6 mm, and with the corresponding size along the y direction of 0.5 and 0.7 mm. The maximum length L reached 6 mm. The injecting contacts were formed on the faces perpendicular to the z axis. The lower n^+ contact, which injected electrons, also acted as a support, so that it was made of a copper cylinder 2 mm in diameter used to solder the structure to the corner of a copper block. This block was attached to a coaxial rod which was placed inside a cryostat. The copper cylinder supporting the sample and supplying the current was cut in its upper part so that its section along the x axis amounted to 0.5–0.7 mm and this governed the extent of the n^+ contact in this direction. The upper p^+ contact, which injected holes, was oval and its shape was governed by the spreading of the melt in the alloying operation. The location of the $p^+ - n - n^+$ injecting structure on a crystal was varied so that the distance from the edge of the lower contact to the neighboring face of the sample (l_1, l_2) ranged from 0.3 to 5 mm.

The duration of electrical double-injection pulses was 0.5–10 μsec and the repetition frequency was 60 Hz. The luminescence spectra were recorded at different moments by a fast-response germanium photodiode ($\tau \lesssim 10^{-7}$ sec) using gate pulses, whose minimum duration was 0.1 μsec. The spatial distribution of the signal was determined by scanning, with the slit of a prism monochromator, an image of the sample enlarged by a long-focus photographic objective. The sample was moved relative to the slit by a micrometer screw. The luminescence reaching the slit was usually generated in a part of the structure 30–60 μ wide. An improvement in the spatial and temporal resolution of the recorded luminescence spectra unavoidably resulted in a deterioration of the spectral resolution. For this reason it was not possible to record spatially resolved spectra at fairly low injection levels and the spectral resolution did not exceed 1 meV.

EXPERIMENTAL RESULTS

Low-temperature double injection in $p^+ - n - n^+$ structures made of pure germanium is a threshold process because of the S-type current-voltage characteristics.

Injection is accompanied by dissipation of a considerable electrical power in a crystal. This heats the injected carriers strongly, as manifested by broadening of the luminescence lines. However, in spite of the considerable heating of the injected plasma, the radiative recombination in the investigated $p^+ - n - n^+$ structures is of the exciton type.[1] This is in agreement with the experimental data on the optical excitation,[2] according to which free-carrier luminescence lines are not emitted by pure germanium even at liquid nitrogen temperature when only a few percent of the injected carriers are bound into excitons. Experiments indi-

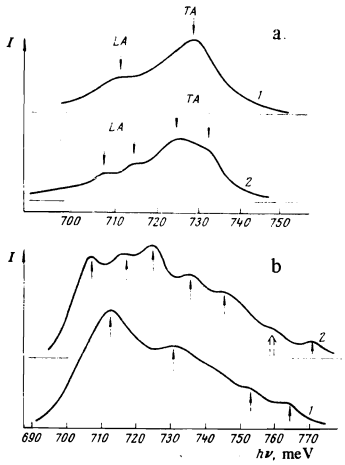

FIG. 2. Luminescence spectra: a) at 2 °K; b) at 77 °K.

cate that these lines appear against the background of exciton lines only when the temperature is raised to $T \approx 100$ °K.

The special nature of the energy band structure of germanium makes it a convenient material for the optical investigation of nonequilibrium processes associated with the relaxation of the energy supplied by external excitation. The localization of the conduction band extrema at the edges of the Brillouin zone makes the indirect transition accompanied by the emission of a transverse acoustic (TA) phonon forbidden at 0 °K and, therefore, the ratio of the rate of indirect optical transitions accompanied by the emission of this phonon to the rate of transitions accompanied by the emission of a longitudinal acoustic (LA) phonon is a measure of the average electron energy.[3] Since[1]

$$\gamma = I_{TA}/I_{LA} = T[\mathrm{K}]/364, \qquad (1)$$

where I_{TA} is the intensity of the luminescence line associated with the emission of a TA phonon; I_{LA} is the intensity of a luminescence line associated with the emission of an LA phonon; T is the electron temperature.

We found[1] that at helium temperatures the value of γ for the investigated $p^+ - n - n^+$ structures reached values corresponding to $T \approx 1000$ °K, whereas the carrier temperature estimated from the width of the luminescence line was ~40 °K. The anomalously strong rise of I_{TA} was attributed by us to the accumulation of non-equilibrium

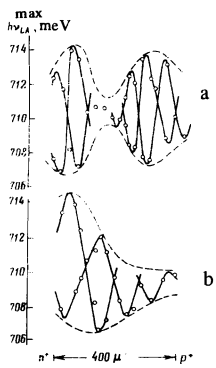

FIG. 3. Coordinate dependences of the position of the luminescence line associated with the emission of an LA phonon obtained at 2 °K ($d = 400$ μ): a) $i = 0.5$ A (in the presence of illumination), $t_p = 8$ μsec, $t_{gate} = 7.0$–7.2 μsec; b) $i = 1.2$ A (in the presence of illumination), $t_p = 1$ μsec, $t_{gate} = 1.4$–1.6 μsec.

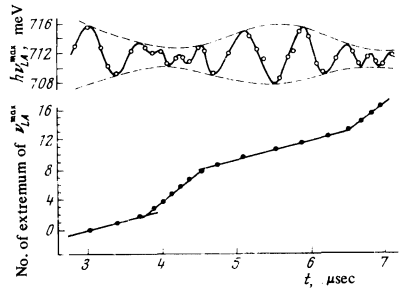

FIG. 4. Dependence of $h\nu_{LA}^{max}$ on time during a current pulse (upper trace) and time dependence of the number of $h\nu_{LA}^{max}$ extrema; $T = 77$ °K, $d = 0.5$ mm, $i = 4$ A, $\Delta t_{gate} = 0.1$ μsec.

quasi-Brillouin TA phonons in a crystal. Then

$$\gamma = {}^1/_{364} T (N_{TA} + 1), \qquad (2)$$

where N_{TA} are the occupation numbers of nonequilibrium TA phonons with $q \lesssim \pi/a$.

We investigated the spatial and temporal distributions of the luminescence emitted from germanium $p^+ - n - n^+$ structures in which the injected electron–hole plasma and phonon system were not in equilibrium at low temperatures. Spatial scanning of the luminescence revealed a strong inhomogeneity of the luminescence. We found that not only the luminescence intensity but also the spectral positions of the luminescence lines and even their number varied periodically from point to point along the direction of the current.

Figure 2a shows two typical luminescence spectra emitted from different parts of a sample at $T = 2$ °K. At certain "points" on a crystal (here, a "point" represents a spatial interval of 40 μ), which formed a regular sequence, we observed the usual luminescence spectra due to transitions accompanied by the emission of LA and TA phonons (spectrum 1). At other points each of the luminescence lines was split into two components (spectrum 2). The splitting varied from point to point. However, the points with the maximum splitting formed a regular sequence. The splitting of the luminescence lines, including the short-wavelength lines associated with the absorption of TA and LA phonons, was also observed at liquid nitrogen temperature (Fig. 2b).

Figure 3 shows the positions of the luminescence lines accompanied by the LA phonon emission ($h\nu_{LA}^{max}$) as a function of the coordinate along the current at $T = 2$ °K. We can see that $h\nu_{LA}^{max}$ oscillated in space giving rise to a beat pattern. The oscillation nodes were the spectra with unsplit lines (1 in Fig. 2a) and the antinodes were the spectra with maximum line splitting (2 in Fig. 2a). It is clear from Fig. 3 that the split lines became transposed after passing through a node: the long-wavelength line switched to the short-wavelength position, and vice versa. It was not always possible to resolve the two split lines in the spectra. For example, in samples in which the current was directed along the [111] axis at 77 °K only one of the split lines predominated and was well resolved. This made it possible to study one of these antiphase oscillations but with a greater precision.

Figure 4 shows the time dependence $h\nu_{LA}^{max}(t)$, re-

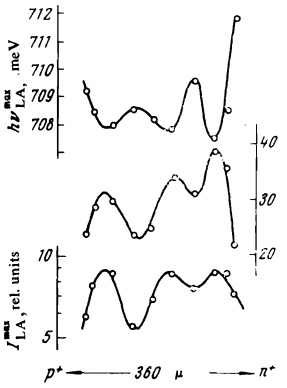

FIG. 5. Coordinate dependences of $h\nu^{max}_{LA}$, I^{max}_{LA}, and T_e at 4.2 °K; $d = 360\ \mu$, $i = 2$ A (in the presence of illumination), $t_{gate} = 1.4$–$1.6\ \mu$sec, $t_p = 1\ \mu$sec.

flecting the changes in the positions of the luminescence lines emitted from a particular region of a $p^+ - n - n^+$ structure during a current pulse of direction $\mathbf{i} \parallel [111]$ at 77 °K. This figure includes also the time dependence of the number of an extremum $h\nu^{max}_{LA}$ showing that the oscillations of this number were periodic in time. Clearly, both $h\nu^{max}(t)$ and $h\nu^{max}(x)$ oscillated giving rise to a beat pattern. This behavior of $h\nu^{max}(x, t)$ indicated that an oscillatory process took place in the investigated $p^+ - n - n^+$ structure and it was due to the interference of two waves with similar frequencies, which altered greatly the energy spectrum of the injected carriers. The maximum long-wavelength shift of the luminescence lines was independent of the current, beginning from the minimum value at which the luminescence spectrum could be recorded; it was also independent of the temperature of a crystal. The position of the line associated with the emission of an LA phonon was then ~ 707 meV at helium and nitrogen temperatures. The smallest values of $h\nu^{max}(x)$ and $h\nu^{max}(t)$ always corresponded to the highest carrier temperatures estimated from the width of the luminescence lines (whenever possible) and also from $\gamma \sim T[N_{TA}(T) + 1]$.

Figure 5 shows the coordinate dependences of $h\nu^{max}_{LA}$ and of the carrier temperature T_e deduced from the short-wavelength wing of the dominant luminescence line associated with the emission of a TA phonon, and also of the intensity I^{max}_{LA} obtained at 4.2 °K for a small current through one of the samples. In this case the minima of the energy positions of the lines corresponded not only to the maxima of T_e but also to the maxima of the intensity of the luminescence associated with the emission of an LA phonon. In most cases at helium temperature and in all cases at 77 °K the value of I^{max}_{LA} oscillated in phase with $h\nu^{max}$. The results obtained at 77 °K are shown in Fig. 6. The variation of γ in antiphase with $h\nu^{max}_{LA}$ (Fig. 6) indicated that the plasma temperature increased as the luminescence lines shifted toward longer wavelengths. The monotonic rise of the average value of γ with the coordinate between p^+ and n^+ reflected the rise of the average carrier temperature in the ambipolar drift direction during a current pulse, as demonstrated directly in Fig. 6.

All the observed oscillations of the luminescence intensity and spectral distribution were smeared and disappeared completely when the spatial or temporal resolution or the focusing deteriorated. Thus, the natural tendency to try and obtain the maximum signal by weakening the sharpness of the focusing resulted first in the disappearance of the high-frequency oscillations and then of the low frequencies (beat frequency). Moreover, integration of the spatially inhomogeneous luminescence yielded a definite conclusion on the energy spectrum of the recombining carriers. The integrated spectrum summed the luminescence of several spatial or temporal periods, and it was dominated by the transitions with photon energies for which the intensity was highest during a period. This was why the information on the long-wavelength shift of the energy spectrum of carriers was lost from the integrated spectrum obtained at liquid nitrogen temperature.

The exact determination of the parameters of the waves whose interference resulted in beats was somewhat difficult and sometimes simply impossible. The problem was that in the case of beats the distribution of the nodes and antinodes in the interference pattern was such that two oscillation periods were observed directly (Fig. 4) and these differed from the periods of the interfering waves. The difference between these periods was a function of the similarity of the interacting waves and of the ratio of their amplitudes. In exact determination of the wavelengths (frequencies) of the interfering waves we have to know the beat period and the number of oscillation extrema within this period. For example, if λ_1' and λ_2'' are the wavelengths of the interfering waves, λ_b is the spatial beat period, N is the number of extrema of the measured quantity inside the beat period, and m_1 and m_2 are integers, then

$$\lambda_b = m_1\lambda' = m_2\lambda'', \quad m_1 + m_2 = N. \tag{3}$$

Under experimental conditions N may assume different but always odd values. This means that $m_2 = m_1 + 1$ and $N = 2m_1 + 1$ so that

$$\lambda' = 2\lambda_b/(N-1), \quad \lambda'' = 2\lambda_b/(N+1). \tag{4}$$

However, it was possible to determine λ_b with the required precision only in some cases. A comparison of the exact values of the oscillation periods found by this method with those deduced directly from the slopes of the dependences $N_{extr}(x)$ or $N_{extr}(t)$ (Fig. 4) indicated that in this case the difference was small (10–30%) and the nature of the dependences on the thickness of a crystal, current, temperature was the same. This made it

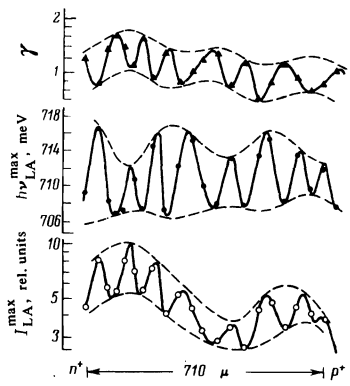

FIG. 6. Coordinate dependences of $h\nu^{max}_{LA}$, I^{max}_{LA}, and γ at 77 °K; $d = 0.71$ mm, $i = 1.1$ A, $t_p = 3\ \mu$sec, $t_{gate} = 2.7$–$2.9\ \mu$sec.

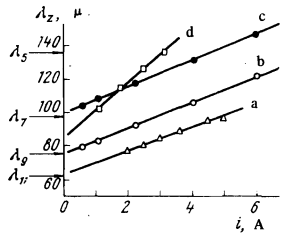

FIG. 7. Dependences of the wavelengths of generated waves on the current: a) λ_{sh} (short-wavelength mode), $d = 0.34$ mm, $T = 4.2$ °K; b) λ_{sh}, $d = 0.34$ mm, $T = 77$ °K; c) λ_{lg} (long-wavelength mode), $d = 0.34$ mm, $T = 77$ °K; d) λ_{sh}, $d = 0.71$ mm, $T = 77$ °K.

possible to use approximate values of the wavelengths and frequencies in qualitative analysis.

The parameters of the interfering waves, whose interaction with carriers changed so greatly the nature of radiative recombination in $p^+ - n - n^+$ structures, varied with the conditions. When the current was increased, the wavelengths of the interfering waves increased and for a fixed current the wavelength increased with the crystal thickness and temperature of the medium (Fig. 7).

The luminescence wavelengths changed also in the process of establishment and decay of a steady-state nonequilibrium conductivity. Measurements were made of the wavelengths of the interfering waves as a function of time, measured from the end of an injection pulse (Fig. 8). The values relaxed to those typical of zero injection level, found by extrapolation of the steady-state values of $\lambda_z(i)$ to zero current $i = 0$ (Fig. 7). The relaxation $\lambda_z(t)$ at times $t > t_p$ (t_p is the pulse duration) occurred at a rate governed by the injected carrier lifetime.

Scanning of the luminescence emitted from the investigated $p^+ - n - n^+$ structures at right-angles to the drift demonstrated that again there was an oscillatory variation resulting in a spatial and temporal inhomogeneity of the radiative recombination. The identification of these oscillations was facilitated by preparing and investigating special samples in the form of long rectangular slabs with injecting $p^+ - n - n^+$ structures (Fig. 1). The luminescence spectra emitted from different parts of such structures, as recorded by scanning along the z and x axes, were identical with the spectra obtained at various points in the current-flow region, some of which are shown in Fig. 2. In spite of the con-

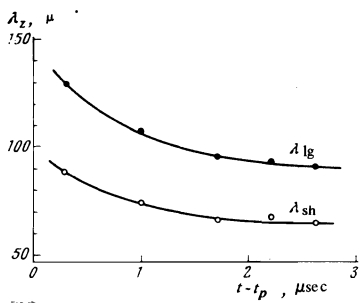

FIG. 8. Time dependences (for $t > t_p$) of the wavelengths of the generated waves; $T = 77$ °K, $d = 0.5$ mm, $i = 6$ A, $t_p = 1$ μsec; λ_{sh} and λ_{lg} were found from the slope of the coordinate dependence of the number of an extremum of the position of a luminescence line maximum.

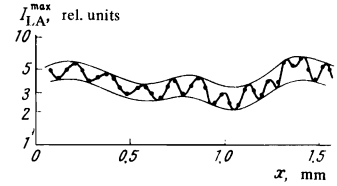

FIG. 9. Dependence, on the coordinate x, of the luminescence intensity and the maxima of the lines associated with the emission of an LA phonon at 77 °K; $d = 0.36$ mm, $t_p = 3$ μsec, $t_{gate} = 2.7-2.9$ μsec, $i = 6$ A.

siderable distance from the injection point (up to 5 mm), not only the width of the luminescence lines and the ratio of their intensities but also the maximum long-wavelength shift (amounting to ~ 6 meV) were the same. Moreover, the periods of the oscillations of $h\nu^{max}(z)$ and $I^{max}(z)$ along the z axis were the same for different parts of a given structure.

All this indicated that the perturbations in the bulk of a $p^+ - n - n^+$ structure propagated without significant attenuation along the x axis. Scanning of the luminescence along this coordinate revealed an oscillatory process responsible for this energy distribution of the external excitation.

Figure 9 shows the distribution, along the x axis, of the intensity of the luminescence line associated with the emission of an LA phonon at 77 °K for a part of the sample separated by 1–2.5 mm from the edge of the injecting structure. The nature of this distribution indicated that a standing wave, formed as a result of interference of the waves traveling along the x axis, was established at right-angles to the drift direction. The amplitude of the standing wave along the x axis was the same as the amplitude of the oscillations in the drift direction so that the position of the maximum of the luminescence line associated with the emission of an LA phonon still oscillated within the energy range 707–718 meV. The minima of $I_{LA}^{max}(x)$ at 77 °K corresponded to the minima of $h\nu_{LA}^{max}(x)$.

The dependence $h\nu^{max}(t)$, found by recording the time dependence of the luminescence intensity at a point with a fixed value of x, was similar to the dependence $h\nu^{max}(t)$ at $z = \text{const}$, shown in Fig. 4. The similarity of these dependences was not only qualitative but also partly quantitative: in both cases the beat wavelength was the same. The only difference was that the high-frequency period T_x along the x axis could be up to 1.5 times greater than the period T_z.

The dependence I_{LA}^{max} shown in Fig. 9 was obtained from the luminescence spectra recorded at different "points" on the x axis at intervals of 0.05 mm. It was practically impossible to obtain this pattern for the whole 5-mm long sample since each spectrum took 15 min to determine; this was particularly true at liquid helium temperature. However, we found that complete information on the oscillation field at right-angles to the drift direction could be obtained even when the complete pattern was not recorded: it was sufficient to follow the envelope of the oscillatory changes in the luminescence intensity over a certain spectral range.

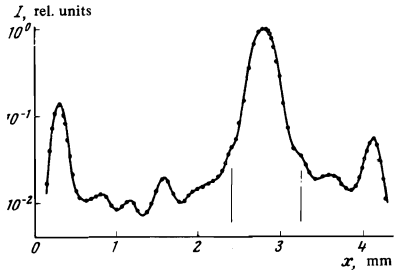

FIG. 10. Spatial distribution of the luminescence intensity at 77 °K in a sample $L = 3.9$ mm long and $d = 0.36$ mm thick. The vertical lines identify the edges of the n^* contact.

This could be done by reducing the spatial and temporal resolution by increasing the monochromator slit width.

We recorded the spatial distribution of the luminescence when the monochromator slit received radiation within the photon energy range 710–715 meV from parts of a sample ~ 150 μ long (Fig. 10). In this procedure the oscillations with a short spatial period, shown clearly in Fig. 9, were not resolved and only the long-wavelength oscillations corresponding to the envelope of Fig. 9 were recorded.

It was interesting to note the rise of the luminescence intensity at these wavelengths at the two ends of the sample. The intensity maxima at the boundaries between the investigated structures and the ambient medium were observed in all cases but the amplitudes of these maxima oscillated with the distance between the $p^+ - n - n^+$ structure and the corresponding edge of the crystal.

There were also two other points in a sample at which there was always a luminescence maximum: these were the edges of the lower (supporting) contact. Sometimes one of these maxima was absolute. This was observed when the upper contact was of much smaller area than the lower one and when one of its edges coincided with the edge of the lower contact. In this case the absolute maximum of the luminescence was observed at the other edge of the lower contact. However, in most cases the absolute luminescence maximum was within the current-flow region and the boundaries of the lower contact corresponded to relative luminescence maxima as shown in Fig. 10.

The intensity of the luminescence at a boundary with the ambient medium I_0 could be represented by the ratio of this intensity to that at the edge of the lower contact I_c nearest to the boundary in question. The distance between these points was the length l whose variation altered harmonically the intensity of the luminescence at the boundary of the sample.

Figure 11 shows the dependence, on l, of the relative intensity of the luminescence emitted at the boundary

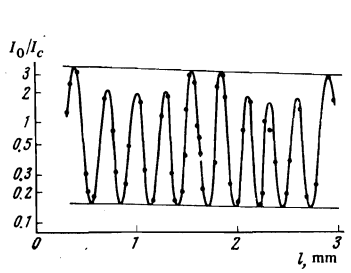

FIG. 11. Dependence of I_0/I_c on the resonator length l.

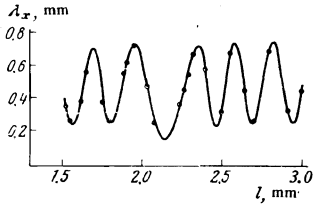

FIG. 12. Dependence of the oscillation period $I(x)$ on l.

between a structure made of a plate $d = 0.36$ mm thick and liquid nitrogen. The dependence obtained was a typical interference pattern which, in this case, appeared due to the reflection, from the boundary with liquid nitrogen, of the waves generated in the transverse direction by the $p^+ - n - n^+$ structure. A noticeable feature was a considerable modulation depth. When the distance l from the $p^+ - n - n^+$ structure was changed by just 0.15 mm, the luminescence intensity at the boundary could change by a factor of almost 20.

A characteristic feature of this interference pattern was a weak reduction in the extremal values of I_0/I_c when the distance to the reflecting surface was increased. The slopes of the lines drawn through the extremal values of $\log(I_0/I_c)$ could be used to estimate the exponential decay constant of the carrier density in the transverse direction $n(x)$ bearing in mind that $I(x) \propto n^2(x)$. At liquid nitrogen temperature it amounted to ~ 2 cm.

When the distance from the source of the excited waves to the reflecting face was varied, we found that oscillations were exhibited not only by I_0 but by the period λ_x of the intensity oscillations. This was found (Fig. 12) for a series of samples with $d = 0.36$ mm at 77 °K. Clearly, λ_x did indeed vary in this manner from $\lambda_{x1} = 0.25$ mm to $\lambda_{x2} = 0.7$ mm. This dependence was periodic, as demonstrated by a plot of the serial number of the extrema $\lambda(N_\lambda^{extr})$ as a function of the coordinate, which gave two values of the period: 0.36 and 0.24 mm. This was of course a more refined value of λ_1. The maximum values of λ_x corresponded to integral values of the ratio l/λ_1 and the minimum values of λ_x (with the exception of the $l = 2.16$ mm case) were observed when a half-integral number of values of λ_{x1} fitted within the length l.

The dependence of I_0/I_c on l (Fig. 11) was also periodic along the x axis and the period was $\Delta l_1 = 0.29$ mm. The luminescence intensity peaks at the end surfaces of the crystal were observed whenever the value of l became half-integral multiple of Δl_1 and the minimum values of I_0/I_c corresponded to the condition $l = k\Delta l_1$, where $k = 1, 2, 3, \ldots$. Moreover, a weaker long-wavelength modulation of the luminescence intensity I_0 was observed at the boundary and the period was $\Delta l_2 = 1.38$ mm. The positions of the extrema could then be found from the condition $l = \frac{1}{2}(k - \frac{1}{2})\Delta l_2$. The minima of I_0/I_c corresponded to even natural numbers and the maxima to odd numbers.

Samples cut from a plate $d = 0.6$ mm thick exhibited dependences analogous to those shown in Figs. 11 and 12 but with different parameters. In this case we found that $\lambda_{x1} = 0.3$ mm, $\lambda_{x2} = 0.6$ mm, $\Delta l_1 = 0.4$ mm, and

$\Delta l_2 = 1.12$ mm.

A special feature of the spatial distribution of the luminescence in the transverse direction was the fact that the minima of the envelope $I(x)$ corresponded to points lying approximately half-way between the end face of the sample and the corresponding edge of the n^+ contact. The same points also corresponded to the minima of the envelope $h\nu^{\max}(x)$. The luminescence intensity in the vicinity of these points was correlated with the intensity at the nearest end of the sample, oscillating in phase with I_0. In contrast to the case of propagation of the excited waves along the direction of the carrier drift, when the wavelengths of the excited oscillations depended quite strongly on the current (Fig. 7), no dependence of the current was observed in the transverse direction.

DISCUSSION OF RESULTS

The characteristics of low-temperature radiative recombination in $p^+ - n - n^+$ structures described above can be explained by postulating the generation of large-amplitude acoustic waves by the interaction of low-frequency lattice vibrations with an intense supersonic flux of injected carriers. Since germanium is a covalent semiconductor, carriers interact with phonons via the deformation potential so that the deformation generated by an acoustic wave is accompanied by a periodic fluctuation of the potential energy of carriers. The conduction band of germanium is quadruply degenerate in respect of the energy at the point L and in most cases the deformation acts in different ways on electrons in different valleys, which lifts the degeneracy and shifts the valleys in different directions on the energy scale. It is this lifting of degeneracy which is manifested by the splitting of the luminescence lines in the field of a large-amplitude acoustic wave excited in a crystal. The injected carriers tend to collect in potential minima created by the acoustic wave and this should concentrate the luminescence in these regions. Such an effect is observed in a helium cryostat under special conditions when the carrier temperature is not too high (Fig. 5).

It follows from the experimental results that the carrier temperature is highest in the potential wells. This additional heating occurs because an acoustic wave creates a periodic fluctuation of the potential energy of carriers E and exerts a force $\partial E/\partial z$ on them, so that it can do work on the carriers contributing to their heating. The action of this force is equivalent to the appearance of an effective electric field[4]

$$\mathscr{E}_{\text{eff}} = \frac{1}{e}\frac{\partial E}{\partial z}.$$

If $E = E_0 \sin qz$, the maximum value of the effective field is $\mathscr{E}_{\text{eff}}^{\max} = qE_0/e$. For typical experimental values $E_0 = 6$ meV and $q \approx 10^3$ cm^{-1}, this field is $\mathscr{E}_{\text{eff}}^{\max} = 6$ V/cm. Such a field causes considerable electron heating in germanium.[5]

In spite of the fact that carrier bunching should occur in the potential wells, in most cases these wells correspond to luminescence minima. This paradox is explained by the fact that, as pointed out earlier, radiative recombination occurring in pure germanium down to $T \approx 100$ °K is of exciton nature and the strong rise of the temperature of the carriers which collect in the wells results in intense evaporation of excitons and a consequent local fall in the radiative transition rate. Moreover, we must bear in mind that the density of states of electrons in the regions where the degeneracy is not lifted may be considerably higher than in the potential wells. For example, in the case of compressive deformation, produced by an acoustic wave travelling along the [111] direction when one conduction-band valley moves downward along the energy scale and the three others move upward, the density of states in the lower split-off valley decreases by a factor of 4 compared with the undeformed state. This explains the special feature of the luminescence spectra of samples with the drift direction parallel to the [111] axis, observed at 77 °K, when good resolution is obtained alternately either for the line associated with the lower valleys or for the line due to the annihilation of excitons which are formed from electrons that include those from the upper split-off valleys (Figs. 4 and 6).

The energy splitting of the conduction band valleys by deformation alters greatly the probabilities of intervalley transitions. Thus, in the absence of deformation[6]

$$\tau_{12}^0 = \tau_{21}^0 \sim \exp\{\hbar\omega_{\text{LA}}/kT_e\},$$

where $\hbar\omega_{\text{LA}} \approx 27$ meV is the energy of an LA phonon with $q \lesssim \pi/a$, whereas in the presence of an energy shift of the valleys by an amount E the probability $1/\tau_{21}$ of a transition from the upper to the lower valleys rises by a factor $\{E/kT_e\}$ and the probability of a transition from the lower to the upper valleys decreases because

$$\frac{1}{\tau_{12}} = \frac{1}{\tau_{12}^0}\exp\left\{-\frac{E}{kT_e}\right\}.$$

Under these conditions we have $\tau_{21} \ll \tau_{12}$ for $E/kT_e \gg 1$ and, if $\pi/\omega > \tau_{21}$, where ω is the acoustic wave frequency, a considerable proportion of carriers collects in the lower valleys. This accounts for the absence of the luminescence lines associated with transitions from the upper split-off valleys (Fig. 5) in the case of relatively low injection rates at helium temperatures when the carrier heating is not too great. These transitions appear only when the current is sufficiently high so that the lattice is heated. When the electron temperature rises, the difference between τ_{12} and τ_{21} decreases and this results in a more uniform population of the conduction band valleys. At 77 °K the transitions from the upper valleys occur always because then $E/kT_e \sim 1$ and the populations of the valleys are comparable.

Solid-state slabs can act as elastic waveguides.[7] However, only certain harmonic modes can propagate in them without a change in shape and these are called the normal waves. A normal wave is a superposition of an even number of plane traveling waves, each of

which can be transformed into another wave as a result of reflection by the waveguide walls. In the simplest case of a plane infinite slab a normal wave can be regarded as harmonic and travelling along the slab with its front perpendicular to the direction of propagation but, in contrast to plane waves in an unbounded medium, with an amplitude modulated harmonically along the front. The number of nodes of a standing displacement or pressure wave along the height of the waveguide governs the serial number of a normal wave. The behavior of a normal wave of a given number depends strongly on the frequency. Each normal wave can exist in a waveguide at any frequency beginning from a certain critical value. At this critical frequency an integral number of longitudinal or transverse half-waves can be fitted into the thickness of the slab so that a new normal wave is a purely standing longitudinal or transverse wave. In this case the vibrations in a waveguide are in phase throughout the length of the guide and they have a constant amplitude.

The critical frequencies of the acoustic vibrations which can exist in such a resonator are given by the interference condition[8]

$$\tfrac{1}{2}[q_z^+(\omega)-q_z^-(\omega)]d+\theta(\omega)=\pi n, \tag{5}$$

where q_z^+ and q_z^- are the wave numbers of the waves traveling in the direction of the carrier drift and in the opposite direction; d is the distance between the reflecting surfaces; θ is the phase shift on reflection; n is an integer governing the number of a normal wave.

In the absence of interaction between an acoustic wave and carriers, we have $q_z^+=q_z^-=2\pi/\lambda$ and Eq. (5) reduces to the usual condition for the appearance of a standing wave:

$$d=\tfrac{1}{2}\lambda(n-\theta/\pi)=\tfrac{1}{2}\lambda n'. \tag{6}$$

The interaction of acoustic waves with free carriers, manifested by the amplification of these waves alters the wave numbers q_z^+ and q_z^- for $\omega=\text{const}$. This change depends in a complex manner on the drift velocity and diffusion coefficient of carriers, on the lattice absorption of sound,[9] and, therefore, on the current and temperature of the investigated crystal. In this case $q_z^+\neq q_z^-$ and a quasistanding wave is formed.

At frequencies in excess of the critical value the components of the wave numbers of normal waves differ from zero along reflecting planes and this is a consequence of the propagation of energy in this direction. The longitudinal $q_z=\pi n/d$ and transverse, q_x and q_y, components of the wave number $q=\omega/v_{si}$ satisfy relationship (i is the polarization index)

$$q_x^2+q_y^2+q_z^2=q^2. \tag{7}$$

If a crystal is limited along the x and y axes by the dimensions l and b, the boundary conditions have to be satisfied on the surfaces and this leads to quantization of q_x and q_y. Then, $q_x=\pi p/l$ and $q_y=\pi m/b$, where m and p are integers, and the frequency of a normal wave of order (n, m, p) is

$$\omega_{nmp}=\pi v_{si}[(n/d)^2+(m/b)^2+(p/l)^2]^{1/2}. \tag{8}$$

Any one of the indices n, m, and p or any pair among them can vanish.

The vibrations generated in the investigated structures can be described adequately by the above pattern of normal acoustic waves in a three-dimensional rectangular resonator. In fact, as pointed out earlier, these vibrations travel over long distances without a significant change in form and the nature of the modulation of the measured spectral quantities (I, $h\nu^{\max}$) in the direction of the thickness remains independent of x.

The observed beats make it difficult to determine exactly the parameters of the vibrations excited in the drift direction. Nevertheless, having determined [by means of Eq. (4)] the spatial periods of the interacting waves, we can find the modes of the excited vibrations and check the interference condition. The values of the emitted wavelengths found in this way as a function of the current (Fig. 7) reflect the influence of the interaction of acoustic waves with a supersonic carrier flux. A direct confirmation of this effect is the agreement between the rate of relaxation of the wavelengths of the excited vibrations after an injection pulse (Fig. 8) with the rate of relaxation of the current.

Extrapolation of the dependence $\lambda_z(i)$ to zero values of the current i and of the dependence $\lambda_z(t)$ for $t>t_p$ to $t\to\infty$ when the interaction in question tends to zero, gives the values of the wavelengths of the eigenvibrations in the resonator. In fact, we can see from Fig. 7 that the values of $\lambda_z(0)$ found by such extrapolation are close to the values of λ_z obtained from Eq. (6) for odd values of n' and identified on the wavelength scale ($\lambda_5-\lambda_{11}$) for the $d=0.34$ mm case. Hence, it follows that $\theta/\pi\approx m$, where m is an integer. Since the reflection of the waves amplified in a crystal occurs at the contacts, which are made of a material of density higher than that of germanium, the phase shift caused by each such reflection is close to π and, therefore, $m=2$.

It is thus found that in the drift direction of a p^+-n-n^+ resonator two neighboring odd modes of the eigenvibrations are excited and these have fairly high numbers $n=n'+2$. For example, in a resonator with $d=0.34$ mm at liquid helium temperature the ninth and eleventh modes are excited, whereas at 77 °K the seventh and ninth modes are produced. In the case of a p^+-n-n^+ structure with $d=0.7$ mm, the seventeenth and nineteenth modes are excited at liquid nitrogen temperature.

The vibrations excited in the direction of the current are transversely polarized. This is indicated by the fact that if $\mathbf{i}\parallel[100]$, the luminescence lines are split. The splitting should not occur for this orientation of the current in the dilatation and compression field created by a longitudinal acoustic wave because a transverse wave traveling along the [100] direction causes succes-

sive shifts of two conduction band valleys in the downward direction and the other two in the upward direction.

The frequencies of the transverse vibrations generated in the drift direction exceed 10^8 Hz and cannot be resolved under the experimental conditions because of the limitations of the gate pulse (minimum duration 10^{-7} sec). However, time scanning at a fixed point $z = \text{const}$ reveals frequencies close to the fundamental frequency of transversely polarized vibrations, where this frequency is given by Eq. (8) with $n = m = p = 1$. The separation of the spatial z component of the fundamental resonator vibration mode, when half a wavelength fits within the thickness of the slab, is difficult because of the background of high-frequency vibration modes.

The following considerations help to identify the vibration modes excited in the transverse direction. The boundary between germanium and liquid helium or liquid nitrogen is almost perfectly soft because of the large difference between their wave impedances $R = \rho v_s$, where ρ is the density of the crystal and v_s is the velocity of sound. In this case the boundary condition corresponds to vanishing of the pressure at the boundary. Consequently, unperturbed positions of the luminescence lines and, for reasons given above, luminescence maxima are always observed along the x direction near the boundaries of a crystal. Similar spectral characteristics are obtained for the planes passing through the edge of the lower supporting contact. The rigidity of clamping of a crystal at these points means that these planes should be nodal for the displacements created by plane waves traveling in the x direction. The requirement of the cophasal displacement and pressure is satisfied only by transverse waves. In longitudinal standing waves a displacement node corresponds to a pressure antinode and vice versa. Thus, transversely polarized acoustic waves are generated at right-angles to the drift direction.

The acoustic field in a three-dimensional resonator may be very complex not only because of the great variety of possible vibration modes at a given frequency and the presence of several excited frequencies but also because of the interaction between various modes, which results in their coupling. This effect is manifested in the investigated structures and it is decisive in the strong modulation of the luminescence intensity.

It is clear from Fig. 9 that the vibrational motion along the length of a crystal is characterized by the existence of several standing waves. The capture of injected carriers in potential wells, created by each of the waves generated in a $p^+ - n - n^+$ structure, results in the drag of carriers by the waves toward the boundary. Each of the standing waves formed by reflection from the boundary gives rise to a relative maximum of the luminescence intensity near the boundary. When several standing waves are present, the luminescence intensity depends strongly on the phase shift between the interfering waves near the boundary and, consequently, on the relationship between the frequencies.

An analysis of the interference pattern observed when the length of a crystal is varied (Fig. 11) makes it possible to determine the normal wave modes excited by the $p^+ - n - n^+$ structure in the transverse direction. It is found that the extremal values of I_0/I_c are observed for such values of l that the frequency of the transverse vibrations of order (0, 0, p), governed by l in accordance with the expression

$$\omega_{00p} = \pi v_{st} p/l, \tag{9}$$

agrees with the fundamental frequency of the transverse vibrations of the resonator

$$\omega_{111} = \pi v_{st} (d^{-2} + b^{-2} + l^{-2})^{1/2}. \tag{10}$$

The values of

$$l_{\min} = \left(\frac{p^2 - 1}{d^{-2} + b^{-2}} \right)^{1/2}$$

are roots of the equation $\omega_{00p} = \omega_{111}$ and are close to the values of l corresponding to the minima of I_0/I_c. The periods Δl_1 of the oscillations of I_0/I_c determined from the experimental results agree, to within 1%, with the values

$$\Delta l = l_{\min}/(p^2 - 1)^{1/2} = 1/(d^{-2} + b^{-2})^{1/2}.$$

This effect is the consequence of the coupling of the fundamental transverse vibration mode of the resonator to high harmonics of the low-frequency transverse vibrations traveling along the length of the crystal. A similar effect, manifested by a reduction in the acoustic activity of a crystal, is typical of quartz plates and it is explained by deterioration of the resonance characteristics of the coupled vibration modes.[10]

In a similar manner we can show that the long-wavelength modulation of I_0/I_c (Fig. 11) is due to the coupling of the x component of the fundamental transverse vibration mode to flexural vibrations traveling along a sample. In this case the values of l corresponding to the minima of I_0/I_c are close to the values of $l_{\min}$ satisfying the equation

$$\omega_{111} = \omega_{\text{flex}}. \tag{11}$$

According to[11], in the case of a slab clamped at one end and free at the other, we have

$$\omega_{\text{flex}} = (n - 1/2)^2 \pi^2 r v_{sl}/l^2, \tag{12}$$

where v_{sl} is the velocity of longitudinal waves in the material, r is the radius of inertia of the transverse cross section, and n is the wave number. Subject to Eqs. (10) and (12), Eq. (11) reduces to

$$v_{st} (d^{-2} + b^{-2} + l^{-2})^{1/2} = (n - 1/2)^2 \pi r v_{sl}/l^2. \tag{13}$$

It is characteristic that in this case the minima of I_0/I_c correspond to the excitation of even-numbered flexural waves. These even harmonics of flexural waves have the highest probability of coupling to odd

shear waves and, particularly, to a transverse fundamental-frequency wave because in these cases the forces acting on the surfaces perpendicular to the displacements vary in a manner similar to the motion of the ends of the slab.[10]

Equation (12) is valid only for a long thin rod. For example, in the case of quartz it applies if $nb/l < 0.1$. In the case of larger values of nb/l the measured resonance frequencies are somewhat lower than those given by Eqs. (12) and (10). Therefore, it is not surprising that in this case the discrepancy between the period Δl_2 found from the experimental results and that calculated from Eq. (13) is greater than in the shear vibration case and it amounts to ~10%.

Periodic coincidence of the frequencies of the generated flexural and shear vibrations with the fundamental frequency of the resonator, which occurs when l is varied, implies that in the strong interaction case out of the large number of possible vibration modes only those are excited whose frequencies are closest to the fundamental resonance frequency ω_{111}. This is indicated also by the similarity of the periods T_z and T_x found by time scanning. The greatest difference between the frequency of the generated shear vibrations and ω_{111} should be observed for $l = l_{\min} + \Delta l/2$, when

$$\omega_{00p}\left(l_{\min}+\frac{\Delta l}{2}\right)=\frac{\pi v_s p}{l}=\frac{p}{(p^2-1)^{1/2}+1/2}\left(\frac{d^{-2}+b^{-2}}{d^{-2}+b^{-2}+l^{-2}}\right)^{1/2}. \quad (14)$$

The maximum deviation of ω_{00p} from ω_{111} is slight, particularly for large values of l. Similarly, the frequency of the excited flexural waves can only differ slightly from ω_{111}.

The proximity of the frequencies of the vibrations generated by a $p^+ - n - n^+$ structure in the transverse direction to the fundamental frequency of the resonator explains the low-frequency beats, observed in the time scanning experiments, as the difference-frequency oscillations.

The excited flexural and shear waves interact not only with the fundamental resonator mode but also between themselves. The result of the interference between these waves is the oscillatory variation of the standing wavelength in the resonator when its length is varied (Fig. 12). For values of l corresponding to the minimum values of λ_x the hybrid wave is close to the shear form, whereas for values of l such that λ_x is largest, the flexural wave is dominant.

The slow reduction in the extremal values of I_0/I_c observed on increase of the length of a crystal (Fig. 11) is evidence of a strong drag of the carriers injected through the $p^+ - n - n^+$ structure by the acoustic waves excited in the transverse direction. For example, at liquid nitrogen temperature the length in the x direction of the packets of dragged carriers is ~2 cm, whereas the diffusion length is $L_D = (D\tau)^{1/2} \sim 10^{-2}$ cm.

The question arises whether energy considerations allow a change in the potential energy by 6 meV by an acoustic wave under the investigated experimental conditions. According to Conwell,[4] in the case of harmonic variation of the potential energy of carriers in the field of an acoustic wave, $E = E_0 \exp[i(qz - \omega t)]$, the acoustic flux J necessary to create E_0 is given by

$$J = 9\rho v_s^3 E_0^2/2\Xi^2, \quad (15)$$

where ρ is the density of the material, v_s is the velocity of sound in the material, and Ξ is the deformation potential. Substituting the relevant values, we find that $J(E_0 = 6 \text{ meV}) = 7 \times 10^3$ W/cm.[2] For typical sections in the current-flow region the necessary acoustic power is $W = JS \approx 10$ W. This is much higher than the power dissipated in a sample during a pulse with the lowest current when the maximum shift $h\nu^{\max} = 6$ meV is observed.

Estimates of the rate of relaxation of long-wavelength phonons in the presence of a thermal reservoir, obtained using the formulas of Gurevich and Gasymov,[12] show that the lifetime of acoustic phonons with $q \approx 10^3$ cm^{-1} is sufficiently long (even at liquid nitrogen temperature) to be comparable with the repetition period of the injection pulses. Consequently, the power of the amplified acoustic wave should increase from pulse to pulse. Therefore, the value $W_{ac} = 10$ W may be attained.

The weak attenuation of the generated waves explains the very possibility of observation of coherent oscillations $h\nu^{\max}(x, t)$ and $I^{\max}(x, t)$ as a result of summation of repeated periodic luminescence pulses. This can also explain the saturation of the amplitude of the amplified wave, which makes the maximum shift of $h\nu^{\max}(x, t)$ independent of the current. In fact, under these conditions the generation of sound in each subsequent pulse begins from a higher initial level and this should increase the intensity of sound with time right up to the saturation value governed by nonlinear effects when the gain begins to depend on the amplitude of the wave being amplified.[13]

The attenuation (absorption) of the generated acoustic waves could not be determined in our experiments. We can only conclude that the lifetime of these waves is long because for several microseconds after an injection pulse we can detect spatially resolved luminescence spectra and the maximum shift of the energy position of the luminescence lines in the $p^+ - n - n^+$ structure remains practically constant.

The observed generation of normal acoustic waves in $p^+ - n - n^+$ structures is due to the amplification of sound by a supersonically drifting injected carrier flux. The generation of high-numbered normal vibrations in the drift direction is due to an increase in the gain of sound with rising frequency $\omega = \pi n' v_s/d$. The upper limit of n is set by the rise in the losses associated with the absorption of sound by lattice vibrations and carriers when the amplified wave travels opposite to the drift direction. Moreover, a special feature of the generation of sound, which is the accumulation of gain from pulse to pulse right up to saturation, makes it necessary to allow for the damping of the amplified vibrations between the pulses in the direction in which the modes grow in the resonator. The changes in the modes of the excited vibrations observed when a sam-

ple is heated from liquid helium to liquid nitrogen temperature (Fig. 7) is a consequence of the growing damping of acoustic waves by lattice vibrations because the lattice temperature rises.

The authors are grateful to L. M. Novak for preparing the samples.

[1]V. N. Ivanov, M. S. Murashov, and A. P. Shotov, Proc. Eleventh Intern. Conf. on Physics of Semiconductors, Warsaw, 1972, Vol. 1, publ. by PWN, Warsaw (1972), p. 170.
[2]J. R. Haynes and N. G. Nilsson, Proc. Seventh Intern. Conf. on Physics of Semiconductors, Paris, 1964, Vol. 4, Radiative Recombination in Semiconductors, publ. by Dunod, Paris; Academic Press, New York (1965), p. 21.
[3]R. J. Elliott, Phys. Rev. **108**, 1384 (1957).
[4]E. M. Conwell, High Field Transport in Semiconductors, Suppl. 9 to Solid State Phys., Academic Press, New York, 1967, (Russ. Transl., Mir, M., 1970).
[5]A. K. Pustovoĭt, Fiz. Tekh. Poluprovodn. **5**, 1989 (1971) [Sov. Phys. Semicond. **5**, 1725 (1972)].
[6]G. Weinreich, T. M. Sanders Jr, and H. G. White, Phys. Rev. **114**, 33 (1959).
[7]M. A. Isakovich, Obshchaya akustika (General Acoustics), Nauka, M., 1973.
[8]V. L. Gurevich and B. D. Laĭkhtman, Fiz. Tverd. Tela (Leningrad) **7**, 3218 (1965) [Sov. Phys. Solid State **7**, 2603 (1966)].
[9]J. D. Maines and E. G. S. Paige, J. Phys. C **2**, 175 (1969).
[10]R. A. Heising (ed.), Quartz Crystals for Electrical Circuits, Van Nostrand, New York, 1946.
[11]J. W. S. Rayleigh, The Theory of Sound, 2nd ed., 2 Vols., MacMillan, London, 1894-6, reprinted by Dover, New York, 1945 (Russ. Transl., Gostekhizdat, M., 1945).
[12]L. É. Gurevich and T. M. Gasymov, Fiz. Tverd. Tela (Leningrad) **9**, 106 (1967) [Sov. Phys. Solid State **9**, 78 (1967)].
[13]V. L. Gurevich and B. D. Laĭkhtman, Zh. Eksp. Teor. Fiz. **46**, 598 (1964) [Sov. Phys. JETP **19**, 407 (1964)].

Translated by A. Tybulewicz

Determination of the density of phonon states of naphthalene crystal from inelastic incoherent neutron scattering

É. L. Bokhenkov, I. Natkaniec,[1)] and E. F. Sheka

Institute of Solid State Physics, USSR Academy of Sciences
(Submitted July 30, 1975; resubmitted November 5, 1975)
Zh. Eksp. Teor. Fiz. **70**, 1027–1043 (March 1976)

The spectra of the inelastic incoherent neutron scattering from a naphthalene crystal were obtained at temperatures 4.7, 80, and 296°K in the energy-transfer region 0–1300 cm^{-1}. The direct and inverse spectral problems are analyzed as mathematical methods for obtaining from experimental spectra information on the density of the phonon states of the crystal. The fundamental difficulties of the method of the inverse spectral problem are discussed. It is shown that no consistent application of this method is possible without an independent solution of the model dynamic problem of the crystal. Under these conditions, the use of the direct spectral problem is more productive. A solution of the direct spectral problem is obtained for the naphthalene crystal. The density of the phonon states of the crystal in the energy range 0–1300 cm^{-1} is determined by comparing the experimental results with the calculations.

PACS numbers: 61.12.Fy, 63.20.Dj

INTRODUCTION

It is widely known that inelastic scattering of slow neutrons in a crystal can serve as the most direct method of studying its phonon spectrum.[1–5] Neutron spectroscopy of phonons, however, which is a realization of this possibility, has not yet become as widely used a method for the studying of the phonon spectrum as, for example, optical spectroscopy. This is caused not only by the complexity of the neutron-spectroscopy experiment and the need for operating with beams of slow neutrons of sufficient density. Greater difficulties are encountered when it comes to extracting information on the phonon spectrum of crystal from the experimental neutron-scattering spectrum. This pertains first of all to the determination of the density of states of the phonon spectra. This question was raised in the literature many times (see[2,3,6–8]), but until recently only the connection between the neutron scattering cross section and the density of the phonon states was considered. It was assumed there that the inelastic scattering cross section (and moreover single-phonon scattering) is obtained from the experimental results. Actually, the determination of the scattering cross section from the experimentally measured spectrum is a rather difficult mathematical problem, so that means of obtaining its solutions must be considered. We shall discuss this problem below for the case of incoherent inelastic scattering. The main conclusions will be illustrated with an analysis of the spectra of neutron scattering in a naphthalene crystal, and a connection will be established between these spectra and the density of the phonon states of the crystal.

1. DIRECT AND INVERSE SPECTRAL PROBLEMS IN NEUTRON-SCATTERING SPECTROSCOPY

In the experimental method of measuring the energy of the scattered neutrons by their time of flight, a